RL-TR-96-274
Final Technical Report
April 1997

PROTEIN-BASED BRANCHED-PHOTOCYCLE THREE-DIMENSIONAL OPTICAL MEMORIES

Syracuse University

Robert R. Birge

APPROVED FOR PUBLIC RELEASE; DISTRIBUTION UNLIMITED.

Rome Laboratory
Air Force Materiel Command
Rome, New York

This report has been reviewed by the Rome Laboratory Public Affairs Office (PA) and is releasable to the National Technical Information Service (NTIS). At NTIS it will be releasable to the general public, including foreign nations.

RL-TR-96-274 has been reviewed and is approved for publication.

APPROVED:

JOSHUA L. KANN
Project Engineer

FOR THE COMMANDER:

JOSEPH CAMERA, Technical Director
Intelligence & Reconnaissance Directorate

If your address has changed or if you wish to be removed from the Rome Laboratory mailing list, or if the addressee is no longer employed by your organization, please notify RL/IRAP,32 Hangar Rd, Rome, NY 13441-4114. This will assist us in maintaining a current mailing list.

Do not return copies of this report unless contractual obligations or notices on a specific document require that it be returned.

REPORT DOCUMENTATION PAGE	Form Approved OMB No. 0704-0188

1. AGENCY USE ONLY *(Leave blank)*	2. REPORT DATE	3. REPORT TYPE AND DATES COVERED
	Apr 97	FINAL, Jan 93 - Jun 96

4. TITLE AND SUBTITLE

PROTEIN-BASED BRANCHED-PHOTOCYCLE THREE DIMENSIONAL OPTICAL MEMORIES

5. FUNDING NUMBERS

C - F30602-93-C-0059
PE - 62702F
PR - 4594
TA - 15
WU - K2

6. AUTHOR(S)

Robert R. Birge

7. PERFORMING ORGANIZATION NAME(S) AND ADDRESS(ES)

Syracuse University
Dept of Chemistry, Center for Science & Technology
111 College Place
Syracuse, NY 13244-4100

8. PERFORMING ORGANIZATION REPORT NUMBER

N/A

9. SPONSORING/MONITORING AGENCY NAME(S) AND ADDRESS(ES)

Rome Laboratory/IRAP
32 Hangar Road
Rome, NY 13441-4114

10. SPONSORING/MONITORING AGENCY REPORT NUMBER

RL-TR-96-274

11. SUPPLEMENTARY NOTES

Rome Laboratory Program Engineer: Joshua Kann, IRAP, (315) 330-4581

12a. DISTRIBUTION AVAILABILITY STATEMENT

Approved for Public Release; Distribution Unlimited.

12b. DISTRIBUTION CODE

13. ABSTRACT *(Maximum 200 words)*

The promise of new architecture and more cost-effective miniaturization has prompted interest in biomolecular optical memories. We examine here the use of the protein bacteriorhodopsin in a branched-photocycle three-dimensional memory. By using a sequential one-photon process, parallel read and write processes can be carried out without disturbing data outside of the irradiated volume. A bench-scale prototype was developed and tested. The prototype used active matrix liquid crystal spatial light modulators, a CCD array detector to monitor the paged data and krypton-ion lasers to provide the irradiation. A variety of data cuvettes were prepared to test various optical geometries and protein environments. The protein was optimized by using both thermal and chemical modifications, resulting in a five-fold improvement in data write efficiency.

14. SUBJECT TERMS

Three-dimensional memories, protein-based devices, bacteriorhodopsin, branched-photocycle volumetric memories, data cuvettes.

15. NUMBER OF PAGES

36

16. PRICE CODE

17. SECURITY CLASSIFICATION OF REPORT	18. SECURITY CLASSIFICATION OF THIS PAGE	19. SECURITY CLASSIFICATION OF ABSTRACT	20. LIMITATION OF ABSTRACT
UNCLASSIFIED	UNCLASSIFIED	UNCLASSIFIED	UL

Table of Contents

List of Figures *(Captions are Abbreviated)*

1. Abstract.

The promise of new architectures and more cost-effective miniaturization has prompted interest in molecular electronics and molecular-based optical memories. Nature has already optimized through serendipitous natural selection some molecules for such applications. We examine here the use of the protein bacteriorhodopsin in a branched-photocycle three-dimensional memory. By using a sequential one-photon process, parallel read and write processes can be carried out without disturbing data outside of the irradiated volume. This final report presents the status of our research and development effort and an overview of what can be realistically expected during the next year of work on this project.

The goals of this contract were to fabricate a prototype protein-based volumetric memory based on the branched-photocycle architecture, test the reliability of the memory and optimize the protein-based memory medium. A prototype bench-scale prototype was developed and tested to investigate the viability of the branched-photocycle architecture based on bacteriorhodopsin. The prototype used active matrix liquid crystal spatial light modulators, a CCD array detector to monitor the paged data and Krypton-ion lasers to provide the irradiation. A variety of data cuvettes were prepared to test various optical geometries and protein environments. The protein was optimized by using both thermal and chemical modifications, resulting in a five-fold improvement in data write efficiency. Reliability problems remain and a 4% error rate in the read operation is observed. This error rate must be improved significantly before this memory architecture can be considered to have commercial potential. A US patent has been submitted and accepted.

2. Rationale and Overview

Bacteriorhodopsin is the light-transducing protein in the purple membrane of *Halobacterium salinarium*, an archaebacterium that inhabits salt marshes [1-5]. This bacterium has survived five mass extinctions during a 3.5 billion year evolutionary period, and has evolved a protein with high photochemical efficiency, photochromic cyclicity and thermal stability [6-12]. A ribbon structure of the protein is shown in Fig. 1. In the native organism, the protein converts light into a proton gradient that is used by the bacterium as a chemiosmotic source of energy.

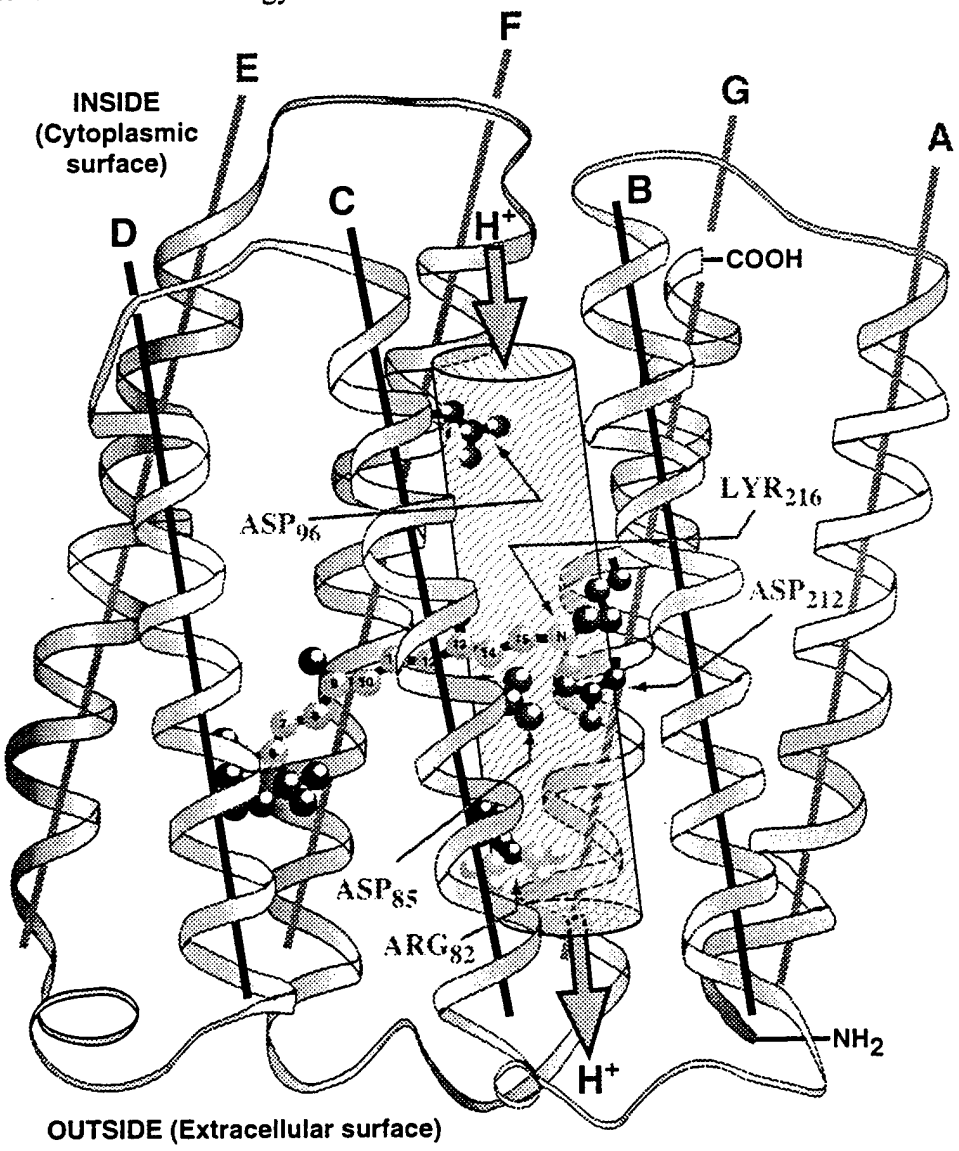

Figure 1. The structure of bacteriorhodopsin is shown using ribbons to represent the seven alpha helical segments that span the membrane. Selected amino acid residues that participate in the proton pumping process are indicated. The shaded gray cylinder (volume $\approx$ 500 Å^3) has a length of about 26 Å and a diameter of about 5 Å and delineates the approximate volumetric region of the proton channel.

Advances in central processor technology have altered the character of computer technology from processor-limited towards memory-limited performance [9]. The overall throughput of many scientific and image analysis problems is now determined primarily by the size and data transfer bandwidths of the random access memory rather than the speed of the central processor unit or the floating point hardware. This situation has generated an increased awareness that new memory architectures providing more cost effective storage capacities, local processing capabilities or data bandwidths should be investigated [13]. Three-dimensional memories store information in a volumetric memory medium and offer as much as a one-thousand fold improvement in data storage capacity for a given enclosure size, although optical and reliability considerations tend to reduce the comparative advantage factor to values closer to 300 [10,11,14,15]. The two most common architectures are based on two-photon [10,13-16] or holographic [17-19] methods. The branched-photocycle architecture explored here is useful because it rigorously excludes photochemistry outside of the doubly irradiated volume, a problem which must be solved before high density volumetric memories can reach their full potential.

The branched-photocycle architecture investigated here was developed in response to problems with the two-photon based architecture. First, high laser intensities are required, which prevent the use of inexpensive laser diodes to write data. This observation is true even though bacteriorhodopsin has one of the largest two-photon absorptivities reported for a broad-band photochromic material [20-22]. Second, unwanted photochemistry invariably occurs along the laser axes, which requires rather complex photochemical cleaning operations to be carried out following the write process [9,23,24]. Third, no protein state which provides for extended lifetime data storage could be created via a direct two-photon process [5]. These three issues suggest that commercialization will not be viable without considerable additional research and development. Fortunately, during the course of these studies we identified a branching reaction of the protein which offers a novel approach to reading and writing data within a three-dimensional polymer cuvette containing the protein.

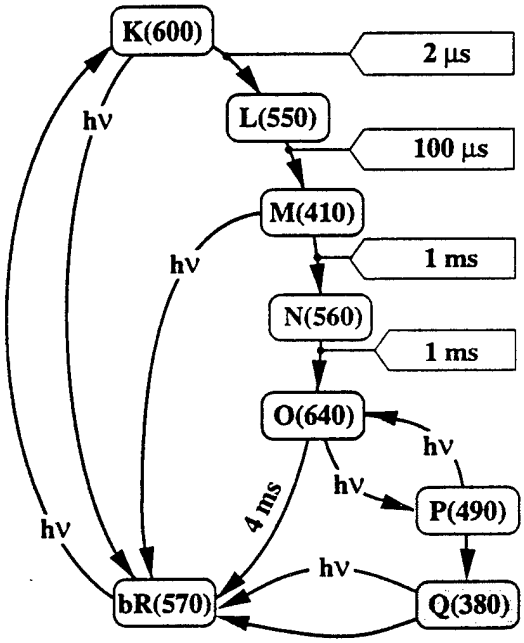

Figure 2. The photocycle of bacteriorhodopsin.

The photocycle of bacteriorhodopsin at 30°C is shown in Fig. 2. The main photocycle is shown in the left-hand portion of the figure and is activated by the primary photochemical event, which converts the resting state, **bR**, into the primary photoproduct, called **K**. The remainder of the photocycle involved thermal reactions which result in reformation of the resting state, **bR**, in about 6-10 milliseconds, depending upon temperature. The last intermediate in the photocycle is called **O**, and this state can be converted by light to form **P**, which subsequently decays to form **Q**. The latter two intermediates are the sole participants in the branching photocycle, which exists as an independent entity from the main photocycle. The key observation here is that this

branching sequence can only be created by a sequential one-photon process. Furthermore, the **Q** state has a lifetime at room temperature of about five years.

Before we discuss the details of the branched-photocycle architecture, it is useful to compare the performance of this architecture relative to the two-photon architecture based on the use of the same protein. A comparison of the sequential one-photon (branched-photocycle) architecture with the simultaneous two-photon architecture based on bacteriorhodopsin is shown in Table I. We note that a majority of the table entries are based on simulations, and thus we must delay final judgment until all the prototyping work is completed. We note, however, that all of the data collected to date indicate that our simulations were either correct or conservative.

Table I. Sequential One-Photon versus Simultaneous Two-Photon Volumetric Memory Architectures Based on Bacteriorhodopsin[a]

Architecture or Property	Two-Photon	One-Photon
Write method	simultaneous 2P	sequential 1P
Molecular representation of zero bit[b]	bR	bR
Molecular representation of one bit[b]	M	P,Q
Parallel write capability	**power/ΔT limited**	*diffraction limited*
Maximum write speed (1024×1024 pixel; per cube)	**~1 MByte/s**	*~10 MByte/s*
Read method	2P photovoltaic	1P paged ΔA
Parallel read capability	***power/ΔT limited***	*diffraction limited*
Maximum read speed (1024×1024 pixel; per cube)	**~1 MByte/s**	*~10 MByte/s*
Bit size in cubic microns (1.6 cm×1.6 cm×2 cm cube)	*~200 μm^3*	**~500 μm^3**
Storage capacity per cube (1.6 cm×1.6 cm×2 cm)	*~2.3 GByte*	**~1 GByte**
Conversions per photon	**~0.0000001**	*~0.0001*
Unwanted axial photochemistry	***5% - 25%***	*none*
Unwanted axial photochemistry after cleaning	***~2%***	*n/a*
Power required	**~ 1 mJ**	*~0.01 mJ*
Lasers required	**pulsed**	*cw or laser diode*
Signal-to-noise ratio	***1.1***	*1.9*
Temperature for >two year storage	***-10°C***	*10 - 40°C*
Optimal operating temperature	***-10°C***	*30°C*
Shelf life of data at ambient temperature	***weeks-months***	*years*

(a) roman† performance neutral; *italics † acceptable or better;*
bold = acceptable but places significant limits on performance;
bold italics = will prevent commercialization unless improved.

(b) In most implementations, both the zero bit and the one bit are represented as linear combinations of **bR** and a second intermediate (**M** in the two-photon memory, and **P:Q** in the sequential one-photon memory). For example, the branched-photocycle memory operates with maximal efficiency by assigning **zero** to [95% **bR** + 5% **P+Q**] and **one** to [85% **bR** + 15% **P+Q**].

3. The Branched Photocycle Architecture

A basic requirement for the implementation of all branched photocycle volumetric memories is the availability of a molecule or light-transducing protein which undergoes a photocycle upon light activation and which has one or more thermal intermediates within the photocycle which can be photochemically converted into a stable species. Orthogonal light beams are used to activate the branched photocycle only at that location within the volumetric memory cell where the two beams cross and the timing between the light beams is appropriate. We anticipate that the branched-photocycle volumetric architecture can be implemented by using a variety of different molecules and light-transducing proteins. As we demonstrate below, however, bacteriorhodopsin has native properties near-optimal for this implementation. Data can be written, read and stored by using the following optical scheme to access the branched intermediates, **P** and **Q**.

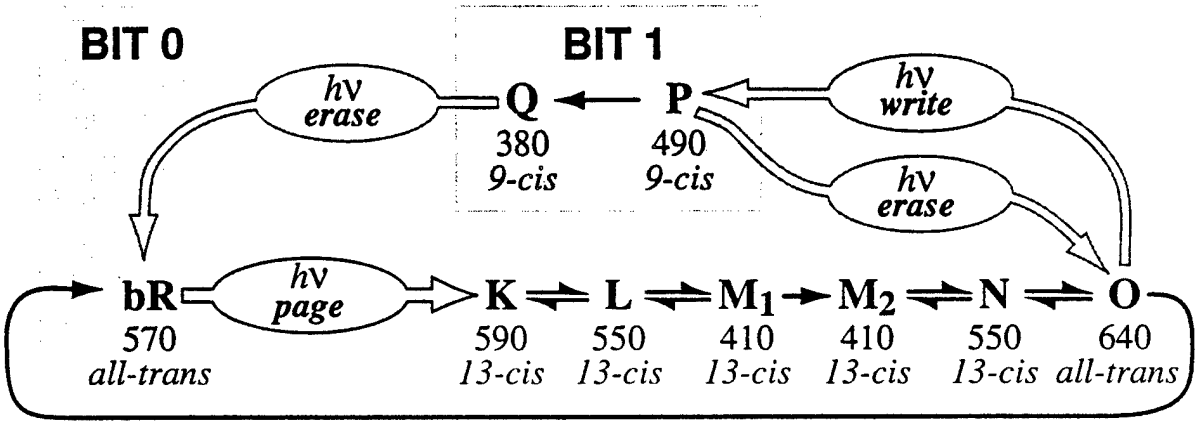

scheme 1

A. Bacteriorhodopsin as an optical AND gate.

Bacteriorhodopsin (MW ≅ 26,000) is the light harvesting protein in the purple membrane of a micro-organism formally known as *Halobacterium salinarium* and commonly called *Halobacterium halobium* [5,8]. The bacterium grows in salt marshes where the concentration of salt is roughly six times higher than that found in sea water. The purple membrane is grown by the bacterium when the concentration of oxygen becomes too low to sustain respiration. The protein, upon the absorption of light, pumps a proton across the membrane generating a chemical and osmotic potential that serves as an alternative source of energy. The fact that the protein must survive in the harsh environment of a salt marsh, where the temperatures can exceed 65°C for extended periods of time, requires a robust protein that is resistant to thermal and photochemical damage. Recent experiments indicate that the protein can withstand temperatures as high as 140°C [7], but under most conditions, denaturation occurs at 80°C. The cyclicity of the protein (i.e. the number of times it can be photochemical cycled) exceeds 10^6 [5,8], a value considerably higher than most synthetic photochromic materials.

The light absorbing chromophore of bacteriorhodopsin is all-trans retinal (vitamin A aldehyde). The chromophore is bound to the protein via a protonated linkage to a lysine residue attached to the protein backbone. The protein bound chromophore carries a positive charge, which interacts elecrostatically with charged amino acids in the protein binding site.

These interactions impart photochemical properties to the chromophore that differ significantly from those observed in the chromophore when in solution. Upon the absorption of light, a rotation around the C_{13}=C_{14} double bond occurs to generate a 13-cis geometry. This process is called a photoisomerization, and in bacteriorhodopsin it is complete in less than one picosecond. The reason for this unusual speed is due to a barrierless excited state potential surface [5]. In this regard, bacteriorhodopsin is a photochemical analog of a high electron mobility transistor (HEMT) device [9].

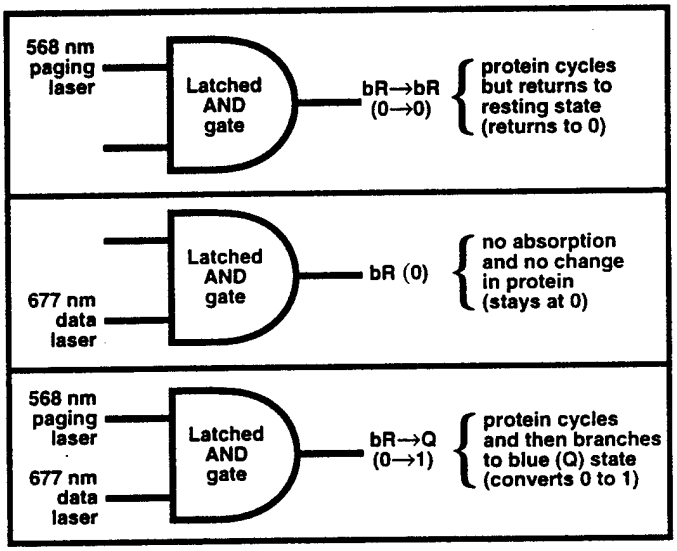

If we assign the **P** and **Q** states as the logical state one, **scheme 1** illustrates the use of the protein as an optically addressed latched AND gate. In other words, the only way to generate a logical one (or in this case, to set bit 1) is to provide two inputs (two photons) at the correct wavelength and timing (see insert at right). This is the key to the rigorous exclusion of unwanted photochemistry and is responsible in part for making the branched-photocycle architecture so attractive in terms of reliability. The quantum efficiency of the primary photochemical event associated with the page selection process is quite high (0.65). This is important in terms of activating an entire page efficiently. The quantum efficiency of the data write process is much lower (0.001 – 0.02), which has both advantages and disadvantages. The advantage is that multiple read operations can be carried out without disturbing the data. The disadvantage is that longer irradiation times (1-4 ms) are required to generate adequate photochemical conversion. The latter problem, however, is circumvented by carrying out as many as 10^6 write operations simultaneously (see below). Note that the two photons are not absorbed simultaneously, and thus this memory operates by a sequential one-photon process, not a simultaneous two-photon process. By activating a page (via the "page" photon) and writing the data (via the "write" photon) by using orthogonal light beams, data can be accessed in three dimensions. The details of these processes are provided in Section 4.

Relatively little is known about the characteristics of the **P** and **Q** states that combine to represent binary state 1. A recent study by Popp et al. provides evidence to indicate that these two states have a 9-cis conformation [12]. Our molecular models of the key states are shown in Fig. 3. By using the same polymer matrix methods as described in our two-photon patent [25], volumetric memory media can be prepared with optimal properties. The details of our current memory media are provided in Section 4.D below.

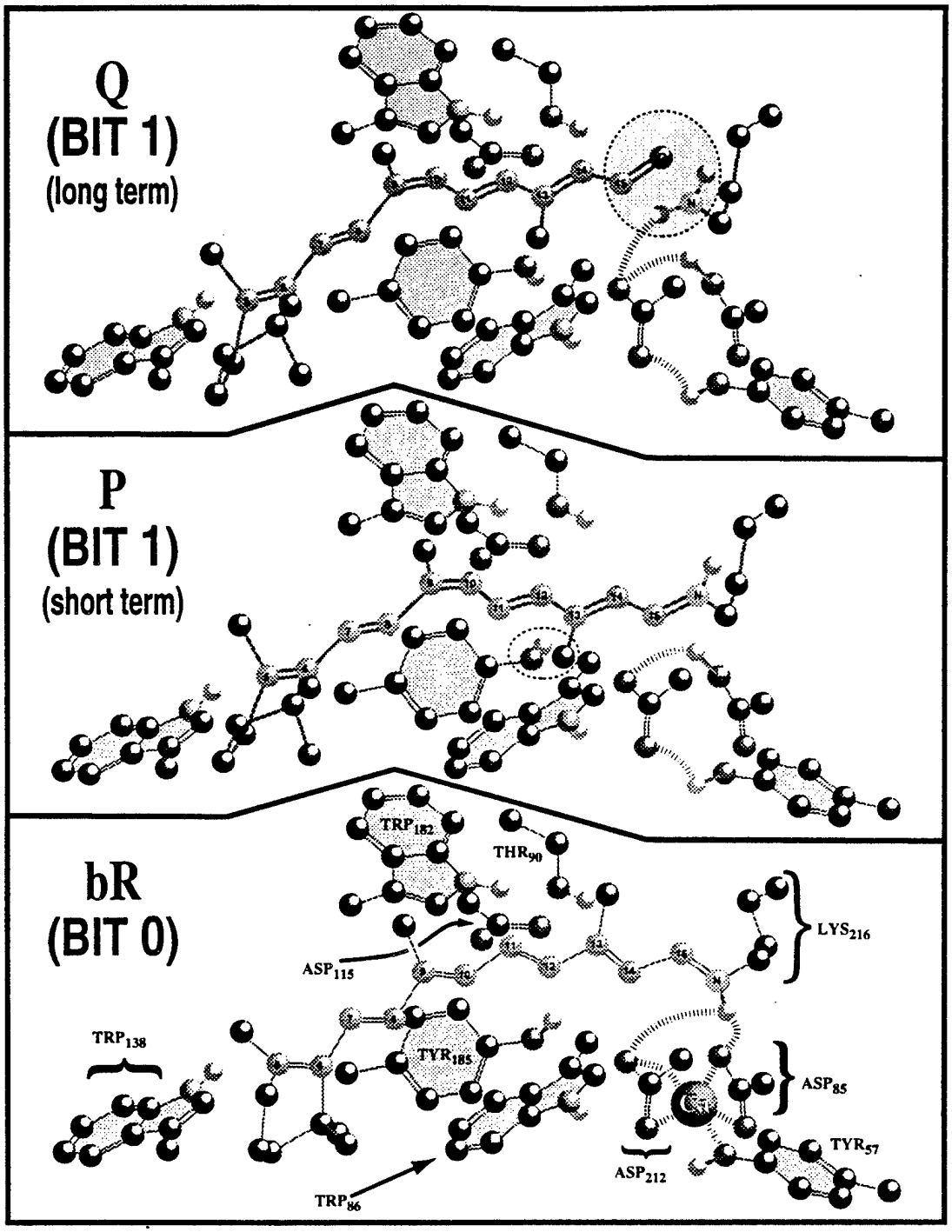

Figure 3. Molecular models of the binding site of bacteriorhodopsin in the resting state (**bR** or BIT 0), the **P** state (short-term BIT 1) and the **Q** state (long-term BIT 1). The location of the calcium ion in **bR** is based on two-photon spectroscopy [22]. The locations of the calcium ion in **P** and **Q** are not known. The chromophore is *all-trans* in **bR** and *9-cis* in **P** and **Q**. The remarkable longevity of the **Q** state is due to the fact that the link to the protein is broken, coupled with the fact that the chromophore remains trapped in the binding site. The only quick way of returning the **Q** state to **bR** is to irradiate it with blue light, which isomerizes *9-cis* back to *all-trans*. This photoisomerization is followed by spontaneous reformation of the chromophore-protein link and regeneration of **bR**.

4. Implementation of the Prototype

In this section we describe the design and fabrication of a bench-scale (Type I) prototype and the methods that are used to write, read and erase data. A schematic diagram of the prototype is shown in Fig. 4, the write and read optical protocols are summarized in Fig. 5 and the absorption spectra of the key intermediates in the main and the branched photocycle are shown in fig. 6.

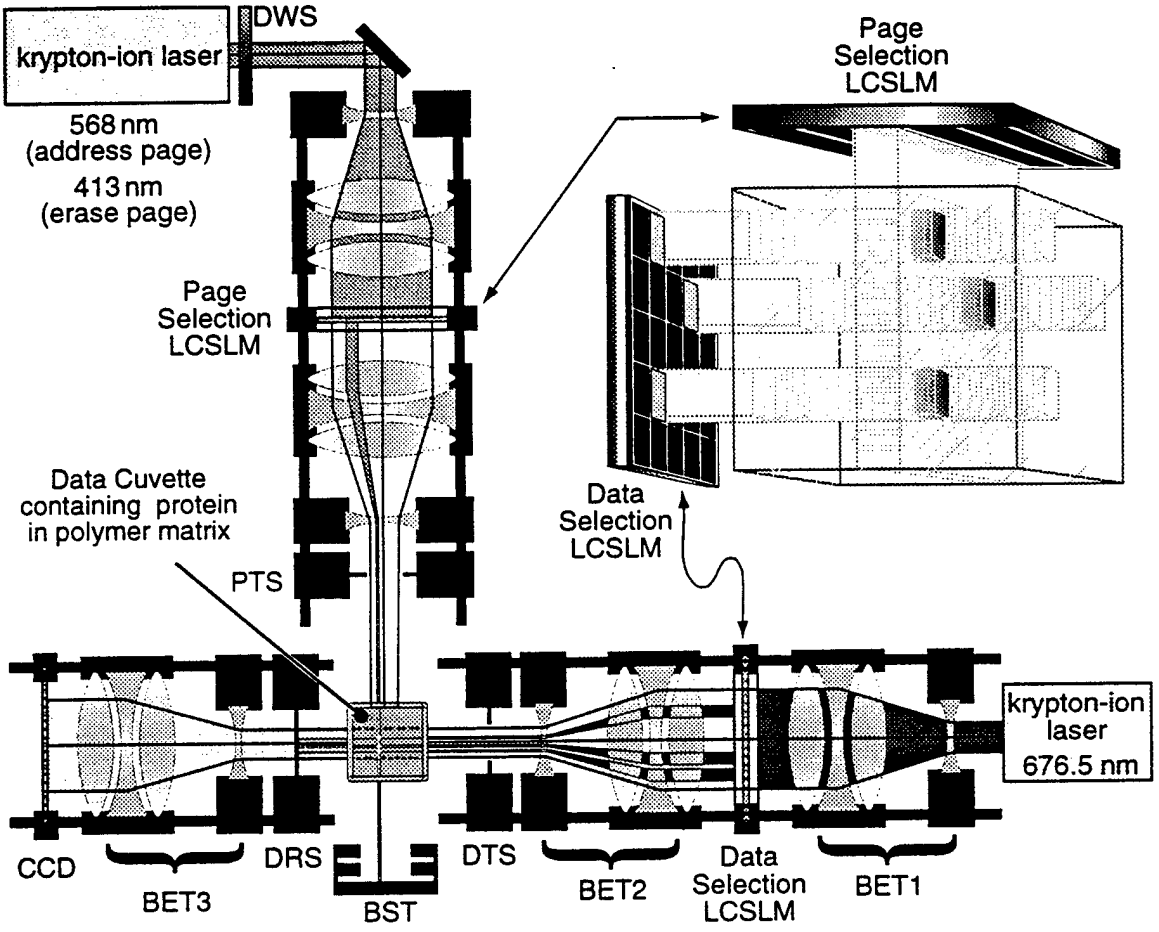

Figure 4. Schematic diagram of the branched-photocycle volumetric memory prototype based on bacteriorhodopsin. Krypton-ion lasers provide the page address (568 nm), data write (676.5 nm), and data erase (413 nm) beams. Active matrix liquid crystal spatial light modulators (LCSLM) provide page selection and data selection with timing mediated via high-speed shutters (PTS, DTS). Beam expanding telescopes (BET) interface the laser beam with the spatial light modulators and a paging beam stop (BST) prevents back reflection of transmitted paging light. The data read shutter (DRS) is closed during write operations to prevent damage to the CCD detector. During the read process, the data selection LCSLM is turned off allowing <0.1% of the light through. The resulting weak beam is sufficient to image the data onto the CCD detector (shutters DTS and DRS are open).

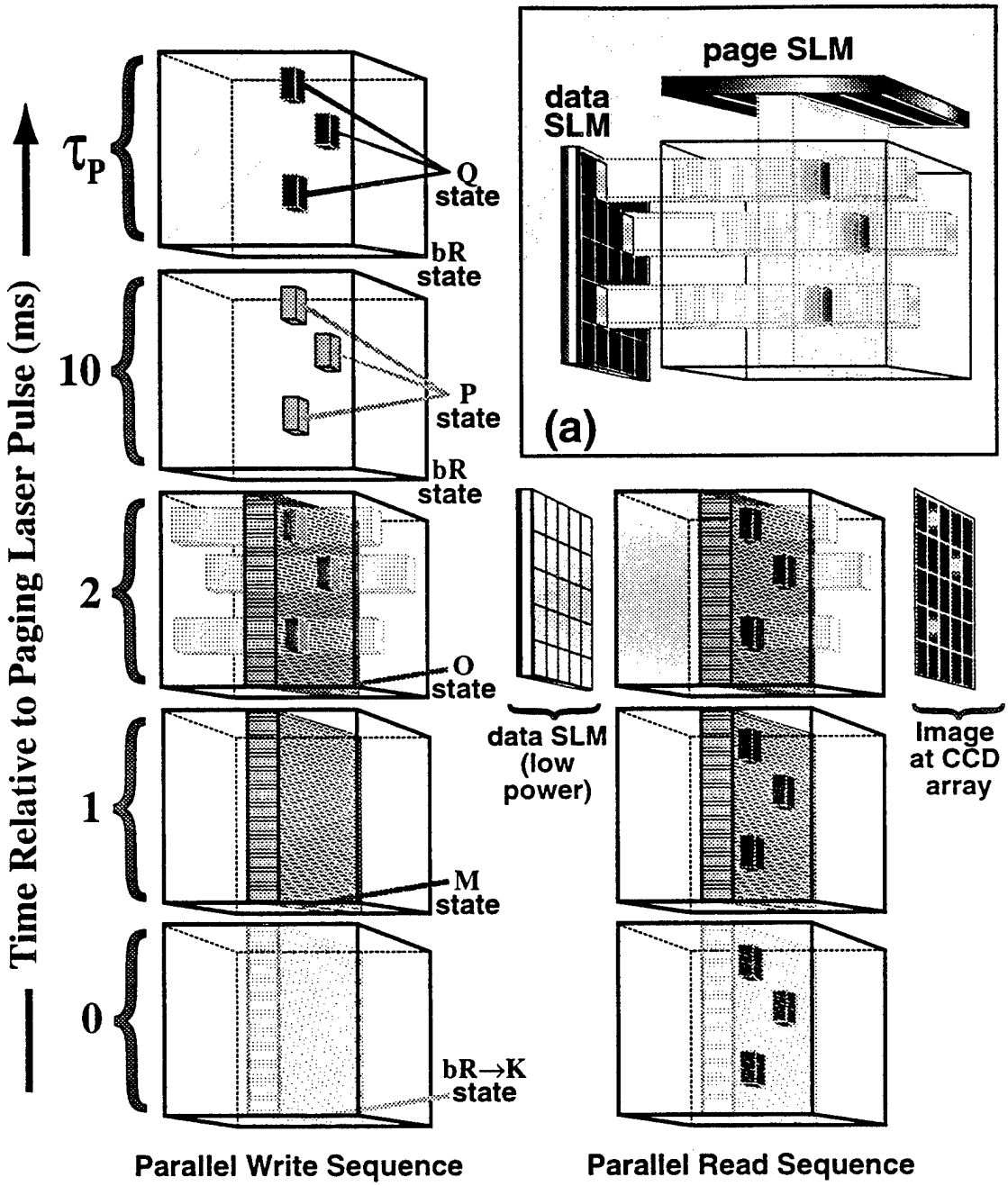

Figure 5. A schematic diagram of the parallel write and read sequences with time progressing from bottom to top. The write sequence (left column) is as follows: (1) turn on the 568nm page beam to activate **bR** photocycle, (2) after ~2 ms, activate appropriate 676.5nm data beams to convert **O** to **P**. The read sequence (right column) is as follows: (1) turn on 568nm page laser to activate **bR** photocycle within paged region only, (2) after ~2 ms, read entire page as an image on the CCD array detector. The basic optical architecture is shown in insert (a).

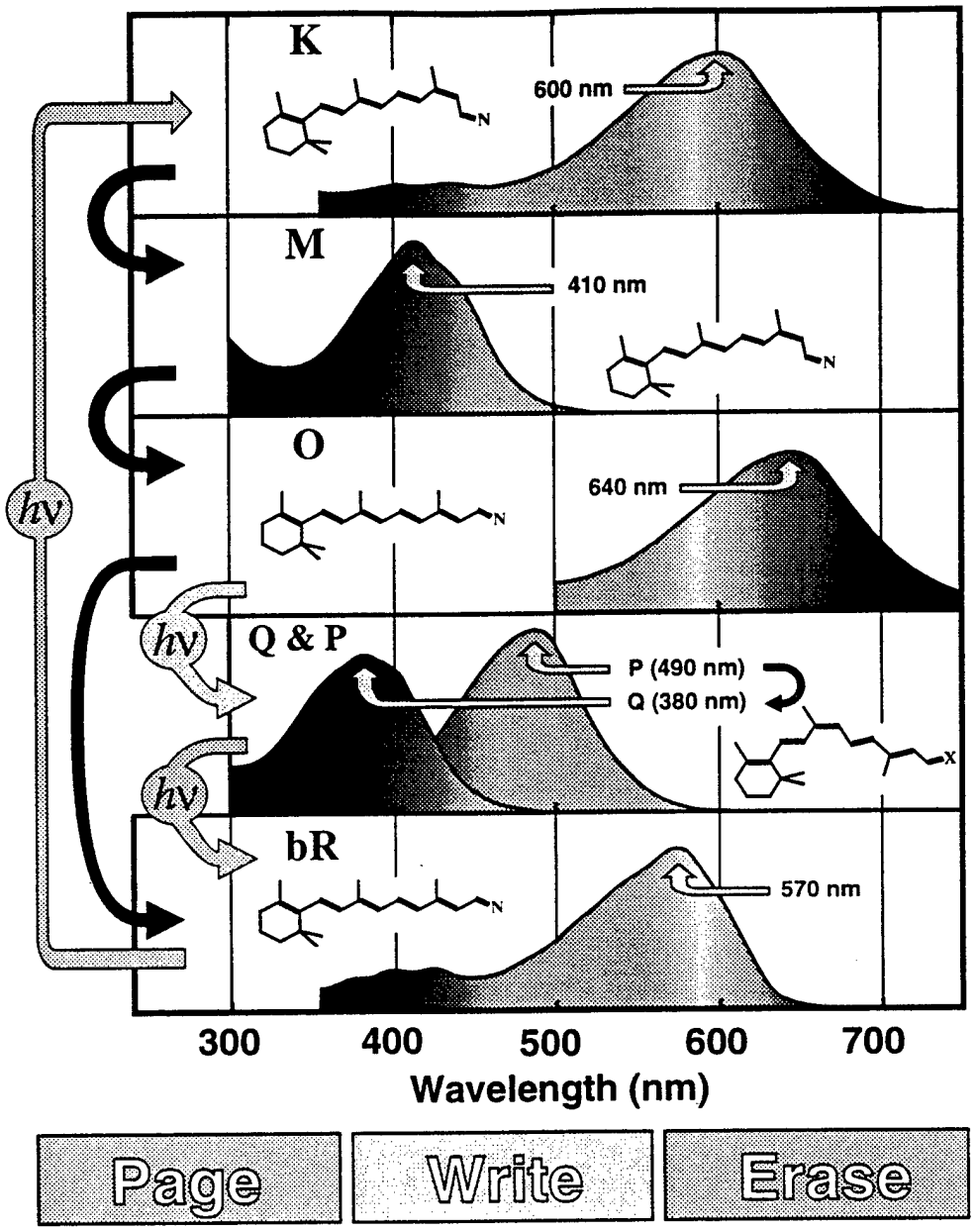

Figure 6. Absorption spectra of selected intermediates in the photocycle of bacteriorhodopsin. Gray arrows indicate light activated processes and black arrows indicate thermal reactions. The structures of the polyene chromophore are shown as inserts [*N* represents nitrogen; *X* represents either nitrogen (in **P**) or oxygen (in **Q**)].

A. Data are written in parallel via a branching reaction.

A parallel write is accomplished by using the sequential one-photon optical protocol shown in Fig. 5. The vertical axis of Fig. 5 charts nominal time relative to the firing of the page addressing (or *paging*) laser. The paging beam (λ = 568nm, Δt < 1 ms) activates the

photocycle of bacteriorhodopsin and after a few milliseconds the **O** intermediate approaches maximal concentration. The data laser and the LCSLM are now activated (λ = 676.5nm, $\Delta t \approx 3$ ms) to irradiate those volume elements into which 1 bits are to be written. This process converts **O** to **P** in these, and only these, locations within the memory cuvette. After many minutes the **P** state thermally decays to form the **Q** state (the $\mathbf{P} \rightarrow \mathbf{Q}$ decay time, τ_P, is highly dependent upon temperature and polymer matrix). The write process is accomplished in ~10 ms, the time it takes the protein to complete the photocycle. This represents an overall write data throughput of ten million characters per second (10 MB/s) for a 1024×1024 data array and two error correcting bits per byte. The wavelengths chosen here are determined by both molecular and laser characteristics and are not optimal for the paging process. Simulations indicate that 600-630 nm paging and 680-700 nm data wavelengths are optimal. Laser diodes with the requisite power (10mW) and beam quality are not yet commercially available.

B. Data are read in parallel by using differential absorptivity.

The read process takes advantage of the fact that light around 680 nm is absorbed by only two intermediates in the photocycle of light-adapted bacteriorhodopsin, the primary photoproduct **K** and the relatively long-lived **O** intermediate (see Fig 6). A parallel read is accomplished by using a differential absorption process as shown in the right column of Fig. 5. The read sequence starts out in a fashion identical to that of the write process by activating the 568nm paging beam. After two milliseconds, the data timing (DTS) and the data read (DRS) shutters are opened for 1ms, but the LCSLM is left off allowing only 0.1% of the total laser power through. A CCD array (clocked to clear all charges prior to opening DTS and DRS) images the light passing through the data cuvette. Those elements in binary state 1 (**P** or **Q**) do not absorb the 676.5nm light, but those volumetric elements that started out in the binary 0 state (**bR**) absorb the 676.5nm light, because these elements have cycled into the **O** state. Noting that all of the volumetric elements outside of the paged area are restricted to the **bR**, **P** or **Q** states, the only significant absorption of the beam is associated with **O** states within the paged region. The CCD detector array therefore observes the differential absorptivity of the paged region, and the paged region alone. This selectivity is the key to the read operation, and it allows a reasonable signal-to-noise ratio even with thick (1–1.6 cm) memory media containing $>10^3$ pages. Because the absorptivity of the **O** state within the paged region is more than 1000 times larger than the absorptivity of the remaining volume elements combined, a very weak beam can be used to generate a large differential signal. The read process is complete in ~10 ms which gives a rate of 10 MB/s. Each read operation must be monitored for each page, and a refresh operation performed after ~1000 reads. While data refresh slows the memory slightly, page caching can minimize the impact.

C. Data can be erased by page or globally.

Data are erased one page at a time by using blue light (the dichroic wavelength selector, DWS, in Fig 4. selects 413 nm). The optimal wavelength for erasing data is ~410 nm, because this wavelength will photoconvert both **P** and **Q** back to **bR** (scheme 1 & Fig. 6). Alternatively, one can clear an entire data cuvette by using incoherent light in the 360 – 450 nm range. The latter option may prove useful for some commercial implementations. A broad-band data clear operation must be carried out in the absence of red light, however, because blue light can activate the photocycle and produce the **O** state. As long as the erasing light is not absorbed appreciably by the **O** state, however, a sufficient population of the **P** and **Q** molecules (bit 1) will be reset to **bR** (bit 0).

As an aside, it is interesting to consider whether a clear operation should be implemented at all. The cost of a data cuvette is relatively small. As noted below, we use

inexpensive plastic cuvettes and the amount of protein that is required to make a single cuvette capable of storing hundreds of megabytes is on the order of milligrams. Because the protein can be produced in mass quantities by using fermentation technology not much different from making beer, some investigators have proposed that the memory be implemented as a WORM device (write once-read many times). An inexpensive bulk eraser device using incoherent blue light could be provided for those wishing to re-use data cuvettes.

D. Preparation of the data cuvette.

Bacteriorhodopsin (BR) is isolated from the bacterium *Halobacterium halobium* (also called *Halobacterium salinarium*) in the form of purple membrane sheets, which consist of the protein suspended in a lipid membrane. Our current strain of *H. halobium* is a variant of S9-P, an enhanced overproducer of bacteriorhodopsin, which is isolated via well-defined procedures described in the literature [22,26]. Purple membrane sheets are suspended in distilled water and stored at 4°C until ready for use. Prior to use, the concentration of BR is adjusted to 10-20 mg/ml.

The cubes used in the branched photocycle volumetric memory are produced by suspending purple membrane in a polymer matrix. The matrix must be sufficiently rigid to encapsulate the membrane and trap it in place, while providing enough moisture to ensure that bacteriorhodopsin retains its full activity. It also must provide a high degree of optical clarity and homogeneity for proper functioning of the optical memory. The polymer matrix must be rigid enough to prevent protein migration, but flexible enough to permit the protein to undergo modest changes in volume that take place during the photocycle. Although we are still looking for improved polymer matrices, to date poly(acrylamide) has shown the most promise.

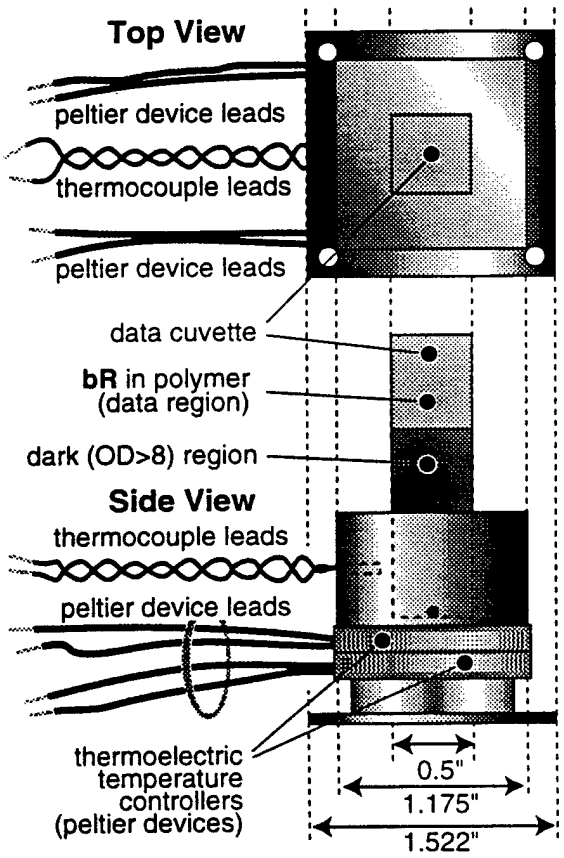

Figure 7. Schematic diagram of the protein data cuvette and holder.

Fabrication of bR-based optical cuvettes (Fig. 7) is accomplished by in situ polymerization of the acrylamide-bR solution. Concentrated purple membrane is added drop-wise to a small volume of 10 % (wt/vol) acrylamide (~2 ml) until the optical density at 570 nm reaches 2-3 absorbance units. The resulting solution is then filtered (5 μ, syringe-type) and sonicated for 1-2 minutes (prolonged sonication can result in vesicle formation, inadequate sonication generates a polymer with too much scattering). At this point the solution is degassed for several minutes, because dissolved oxygen can inhibit the acrylamide polymerization process. Fresh ammonium persulfate solution ($(NH_4)_2S_2O_8$, 1.5% aqueous, w/v) is added to initiate and catalyze polymerization, followed by a small volume of TEMED (N, N, N', N'-Tetramethyl-ethylenediamine) to act as an

accelerator of the polymerization process. The volumes of these two reagents are typically on the order of 75 μL and 10 μL, respectively, per mL of 10 % acrylamide. The solution must be quickly mixed and transferred to a standard fluorescence cuvette before polymerization is fully accelerated; failure to do so will result in optical distortions within the matrix (flows and eddies due to differing rates of polymerization). The rate of polymerization is largely controlled by the concentrations of ammonium persulfate and TEMED. The volumes of these reagents can therefore be adjusted to minimize formation of optical defects in the cube. The total volume of acrylamide/bR solution needed is approximately 1.5 ml.

The acrylamide solution is prepared to be 10% T and 5% C, where T represents the total monomeric concentration of acrylamide, and C represents the concentration of cross-linking agent (bisacrylamide). Addition of a cross-linking agent enables the formation of an actual gel, as opposed to a viscous solution of long polymer chains which would be incapable of encapsulating the purple membrane fragments. The relative proportions of T and C are crucial to the ultimate optical quality of the gel, especially with respect to light scattering. The concentration of cross-linking agent controls the effective pore size, and is generally within the range of 2.5 - 5% (pore size of approximately 20 nm).Addition of too much bisacrylamide (relative to acrylamide) leads to enlarged pore diameters (several hundred nm) and a consequent increase in light scattering [27].

After the cube has gelled, a second acrylamide layer is added. The purpose of this layer is two-fold: primarily, it aids in the reduction of light scattering and reflection which might interfere with the reading and writing processes, and secondly it acts as a filler for the rest of the cuvette, which is then sealed to ensure that it is air-tight. The protocol for fabrication of this layer is as described above, except that enough bR is added so that the solution appears black: deeply colored laser dyes were originally attempted for this purpose, but preliminary studies indicated that they interfered with the polymerization process. The cuvette is filled to about two thirds of its total volume, and is made air-tight by the use of either silicone sealants or a UV-curable optical adhesive. A custom-made base for the cube facilitates permanent sealing of the cuvette, as well as temperature regulation via peltier coolers. The cube base is illustrated in Fig. 7. The cuvette is inserted into the holder, which is equipped with ports for insertion of thermocouples which monitor the temperature and indirectly control the peltier coolers.

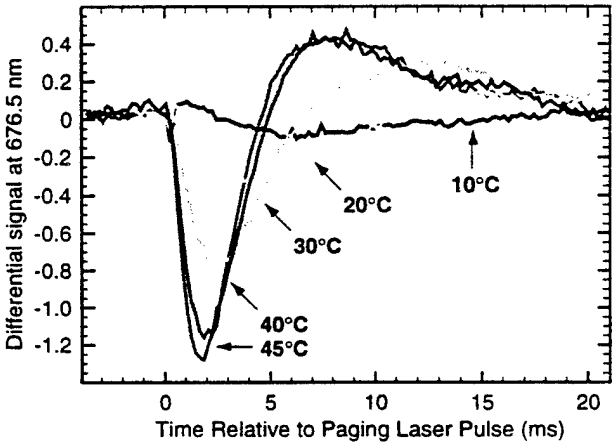

Figure 8. The effect of temperature on the magnitude and the decay time of the differential read signal.

E. The effect of temperature.

Our studies indicate that the signal-to-noise ratio of the read process is highly dependent upon temperature. Furthermore, the probability of writing a one bit is enhanced by increasing the temperature. Both factors are associated with the effect of temperature on the formation of the **O** state. The key experimental results are shown in Fig. 8. The downward peak is associated with the formation of the **O** state, and the consequential

absorption of the 676.5 nm beam by this state. The rise time is associated with the decay of the **O** state, but the fact that it "over shoots" the zero level is due to capacitive effects in the detector array (we are working to eliminate this problem). Note that the intensity of the negative signal as well as the decay of the signal increases with increasing temperature. This observation can be explained by reference to the detailed kinetic analyses of the photocycle carried out by Varo and Lanyi [28,29]. The signal to noise ratio of the read process is proportional to the magnitude of the negative signal divided by the magnitude of the signal fluctuation in the time segment from -2 to 0 ms. The worst-case S/N ratios for the read process as a function of temperature are as follows: 1.5 (10°C), 3 (20°C), 8 (30°C) and 11 (40°C). Other sources of error become dominant in producing read errors at temperatures above 30°C, and hence we have adopted this temperature as the nominal operating temperature of the data cuvette. As noted previous, the temperature of the cuvette is controlled by using thermoelectric heaters (see Fig. 7).

Temperature also affects the timing of the write and read data beams. For optimal writing, the on and off times are given by the following equations,

$$\Delta t \text{ (data beam on)} = 21.8 \text{ ms } T_c(°C)^{-0.7} \qquad (10°C < T_c < 45°C) \qquad (1)$$

$$\Delta t \text{ (data beam off)} = 61.1 \text{ ms } T_c(°C)^{-0.7} \qquad (10°C < T_c < 45°C) \qquad (2)$$

where Δt is the time in milliseconds relative to address beam activation and T_c is the temperature of the memory cuvette in degrees Centigrade. The above relationships are approximate and are limited to pH=7 solution or well humidified polymer environments. The data beam on time is equal to the time at which the signal curve if Fig. 8 reaches half of its minimum value. The data beam off time is equal to the time at which the signal returns to its half-minimum value. These times are appropriate for both the read and write data beam timings, but as noted above, the read process is carried out by using a very low light level. Examination of Eqs. 1 and 2 indicates that the memory can operate more rapidly at higher temperatures, but temperatures above 40°C should be avoided as elevated temperatures decrease the cyclicity of the protein.

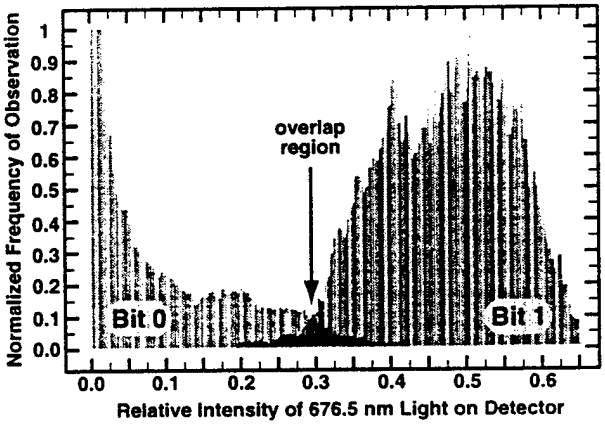

Figure 9. Error during the read process.

F. Reliability

Errors during the read process are being tracked at about 4%, due to overlap in the bit 0 versus bit 1 signals (see Fig. 9). We have identified two principal sources of error. First, the percentage of protein molecules converted from the **O** state to the **P** state during a single bit 0 → 1 conversion is currently about 3%. We must increase this conversion to improve reliability. Second, homogeneity of the data cuvettes must be improved to decrease scattering and refractive misdirection of the laser light.

The optical issues are currently being addressed in collaboration with two companies, TROPEL (60 O'Connor Road, Fairport, NY 14450) and Gradient Lens Corporation (207 Tremont St, Rochester, NY 14608). Both companies have donated their time to this project, and we gratefully acknowledge their support and guidance. We note that their comments, criticisms and suggested modifications in our optical design have not

as yet been implemented. In the final section, we report on protein modifications that have been identified that increase the yield of the **O** state. As of the writing of this final report, these modifications in the protein are being introduced into the data cuvette preparations, and will be reported on in the final report for contract F30602-95-C-035.

6. Protein Modifications to Improve Memory Performance.

During the course of this investigation, we uncovered a chemical method of improving the yield of the **O** state. As noted above, one of the issues regarding reliability is linked directly to **O** state yield, and we have been studying both chemical and genetic methods of improving this variable. One promising approach is site directed mutagenesis, and in particular, the replacement of leucine 93 with tyrosine. This single amino acid substitution greatly increases the yield of the **O** state, but it also increases the lifetime of the **O** state, which slows down the cycle time of the memory. Other mutants are under study, and will be reported on subsequently. This section will concentration on a discussion of organic cation protein analogs, a few of which yield a five-fold improvement in protein performance.

It has long been known that the functioning of light–adapted bacteriorhodopsin ($\lambda_{max} \approx 570$ nm) as a proton pump requires the presence of Ca^{2+} and Mg^{2+} ions which bind at specific locations inside the protein and on the surface [22]. Approximately 3-5 divalent cations are bound to the protein, although the mechanism of the binding remains a subject of debate [30]. Removal of these cations produces what is called the blue membrane ($\lambda_{max} \approx 605$ nm), a protein with a truncated photocycle incapable of vectorial proton pumping. The spectroscopic and photochemical properties of the protein can be restored fully by adding either calcium or magnesium to an aqueous solution of the blue membrane [22,30]. The second high-affinity binding site is primarily responsible for the blue to purple transition [31]. Recent two-photon experiments indicate that this binding site, hereafter referred to as the chromophore-adjacent cation binding site, involves the participation of ASP_{85} and ASP_{212} along with additional stabilization from TYR_{57} and TYR_{185} [22]. This model of the binding site is shown in the bottom diagram of Fig. 3.

We have observed that analog proteins with nearly identical spectroscopic properties and similar photochemical properties can be generated by adding large organic monovalent and divalent cations to the blue membrane [32]. A selection of some of the organic cations that we have studied with respect to protein performance related to the three-dimensional memory are shown in Fig. 10. The spectra of the organic-cation bR analogs are similar to the native protein with absorption maxima within a few nanometers of the native protein. In order to examine systematic variations, the main absorption bands of the protein spectra were fit by using a log-normal distribution function. This procedure fits the band to a skewed Gaussian as a function of the absorption maximum (λ_{max}), full-width-at-half-maximum ($\Delta\tilde{\nu}$) and skewness (σ). The results of the least-squares fits are shown in Fig. 10 for spectra recorded in polyacrylamide gel (the polymer used to make the data cuvettes). As we demonstrate below, the modest shift in absorption spectra do not fully reveal the large changes that were observed in the **O** state kinetics.

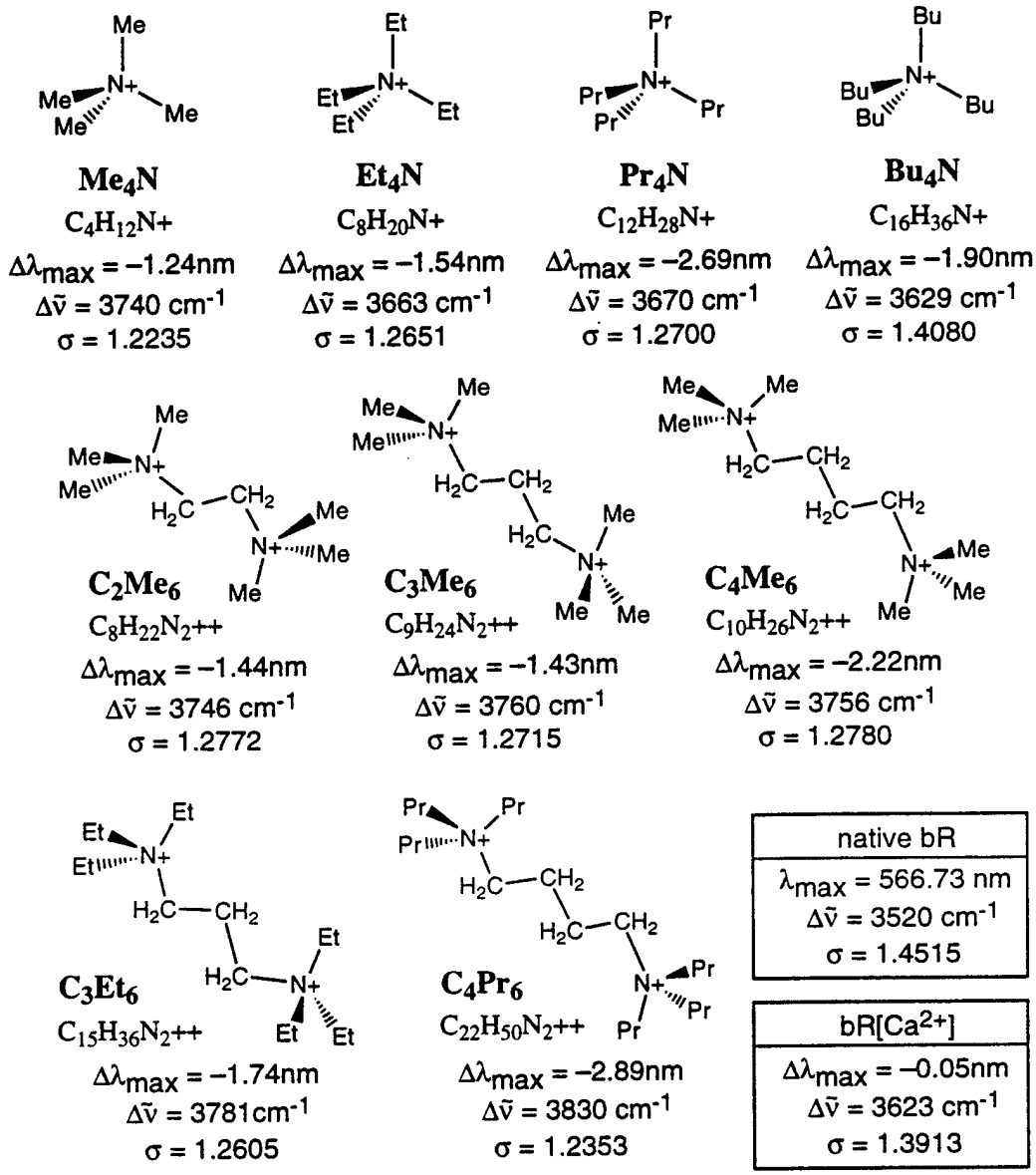

Figure 10. Structure of the quaternary ammonium cations and the spectroscopic properties of the light-adapted analog proteins generated via addition of the organic cations to the blue membrane of bacteriorhodopsin.

A. Preparation of the organic cations.

The dibromoalkanes and trialkyl amines were purchased from Aldrich (cat. nos. 24,065–6, 12,590–3 and 14,080–5) and Fluka (cat. nos. 92260, 90342 and 93240) respectively and were used as received. Acrylamide, N,N'–methylene–bis–acrylamide, azolectin, tris(hydroxymethyl)aminomethane (Tris) and EDTA were purchased from Sigma (cat. nos. A–8887, M–7279, P–7443 ,T–1503 and EDS respectively) and were used without further purification. Ammonium persulfate and $CaCl_2.2H_2O$, purchased from Fisher (cat. nos. A682–500 and C–79 respectively) were of pure grade. Iodomethane and tetramethylethylenediamine were purchased from Aldrich (cat. nos. 28,956–6 and 41,101–9

respectively) and were used as received. Distilled and deionized water (Barnstead E–pure) was used throughout the experiments.

The divalent 'bolaform' cations [$\mathbf{C_nR'_6}$ where n is the number of carbon atoms in the alkyl chain attached between the two quaternary ammonium groups and **R'** references the six identical hydrocarbon groups attached to the two nitrogen atoms, **R'** = CH_3 (**Me**), C_2H_5 (**Et**) or C_3H_7 (**Pr**)] were synthesized from the appropriate dibromoalkane by using the following reaction to form the desired n–alkane–α,ω–bis(trialkylammonium)dibromide:

$$Br(CH_2)_nBr + 2\,\mathbf{R}_3N \xrightarrow[\text{reflux ~3hrs.}]{\text{MeOH}} Br\mathbf{R}_3N(CH_2)_n\mathbf{N}R_3Br \qquad \text{(scheme 2)}$$

where n = 3 or 4 and **R** = CH_3 (**Me**), C_2H_5 (**Et**) or C_3H_7 (**Pr**). The details of the preparation follows a standard method [33]. A two–fold excess of the trialkylamine of choice is added to a methanolic solution of the dibromoalkane and refluxed for about three hours. The product, which is precipitated upon cooling the solution, is filtered off and washed three times with cold methanol. The supernatant is partially evaporated by using a rotary evaporator and a few drops of ether is added before the solution is chilled to form a second batch of the product. The crude product is recrystallized three times from methanol to produce the pure, white–crystalline powder. We discovered, however, that the above procedure is not applicable to the preparation of $\mathbf{C_2Me_6}$. The NMR spectrum revealed displacement of only one of the bromides of 1,2–dibromoethane by trimethyl ammonium. Thus, $\mathbf{C_2Me_6}$ was prepared by the following procedure. A slight excess of methanolic iodomethane is added dropwise into a methanolic solution of tetramethylethylenediamine. The mixture is left to stand for ~1 hour. The crude product which precipitates is filtered off, washed three times with cold methanol and recrystallized three times from methanol to yield the desired white–crystalline product.

B. Photophysical properties of the organic cation analog proteins.

Although the organic cations have an impact on a number of the photophysical properties of the protein, we will concentrate on an analysis of only two properties relevant to this contract. The first is cyclicity, or the number of times the protein can be cycled from the resting state (**bR**) to the branched states (**P & Q**), and then back again to **bR**. The number for the native protein is about 10^5, which means the native protein under normal applications, will function for about five years of normal use. All of the organic cation analogs appear to have a comparably cyclicity with the exception of the large monovalent cation analogs such as $\mathbf{Bu_4N}$. The latter has a cyclicity of about 10^3,which is unacceptable. Further study of this parameter will be carried out during the coming months.

The key property provided by some of the organic cations involves the lifetime and the yield of the **O** state. The experimental results are shown in Fig. 11.

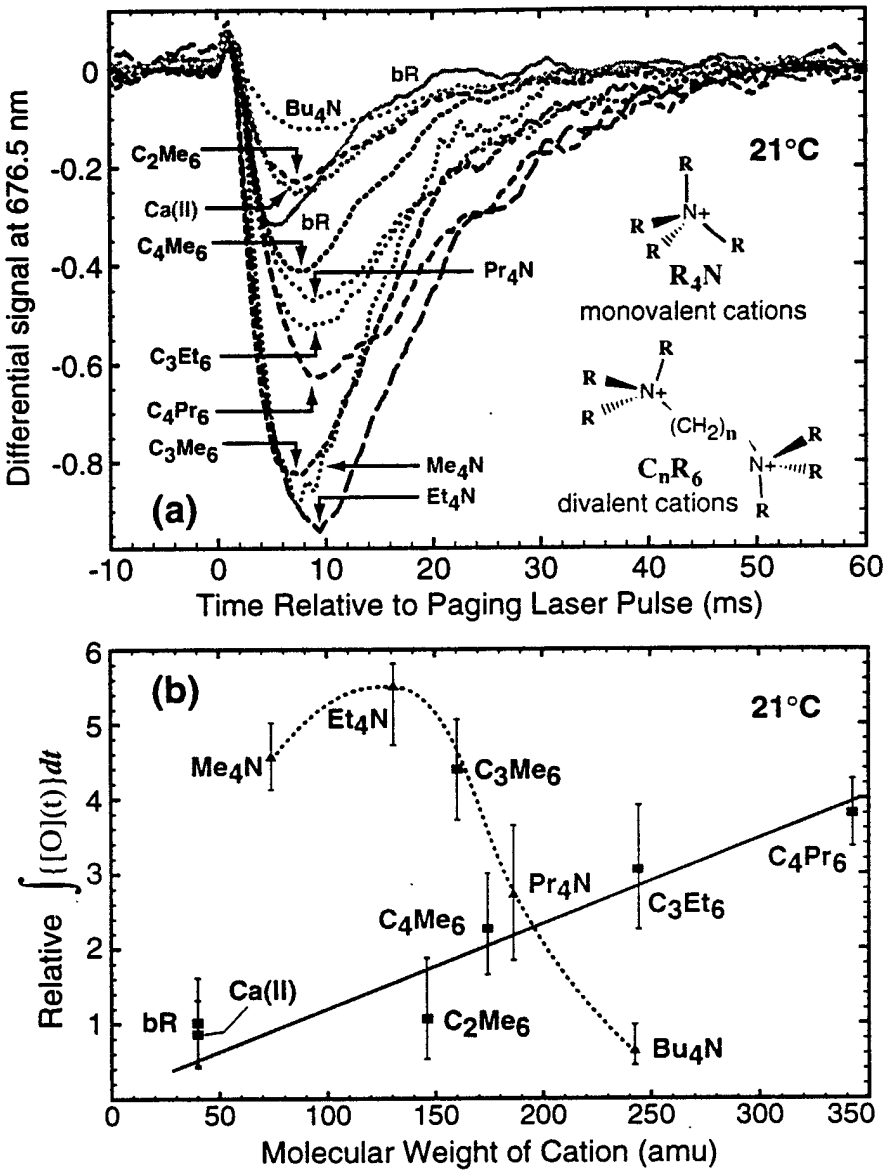

Figure 11. The influence of organic cation size and structure on the formation, decay and yield of the **O** state. Some organic cations enhance significantly the yield and the lifetime of the **O** state. The efficiency of photogenerating the **P** state from the **O** state (i.e., writing bit 1) is proportional to the integral of **O** concentration with respect to time, which is graphed as a function of the cation molecular weight in (b).

The results shown in Fig. 11 indicate that three organic cations generate a dramatic improvement in the **O** state yield (monovalent species **Me_4N** and **Et_4N**, and divalent species **C_3Me_6**; see Fig. 10 for the structures). In particular **Et_4N** produces a 5.4-fold increase in **O** state yield, which translates to a potential improvement of **P** & **Q** formation from 3% to 16%. Our simulations indicate that optimal performance is obtained at approximately 10% conversion, so other organic cations will also be investigated to find the best compromise involving yield, stability and synthetic convenience.

The key advantage of using this chemical approach, as opposed to genetic engineering, is that the extent of the **O** state population and lifetime enhancement can be tailored accurately to achieve a specific goal. This observation follows from the fact that there is a very large number of possible organic cations, and by varying either structure and/or molecular weight, systematic control can be achieved.

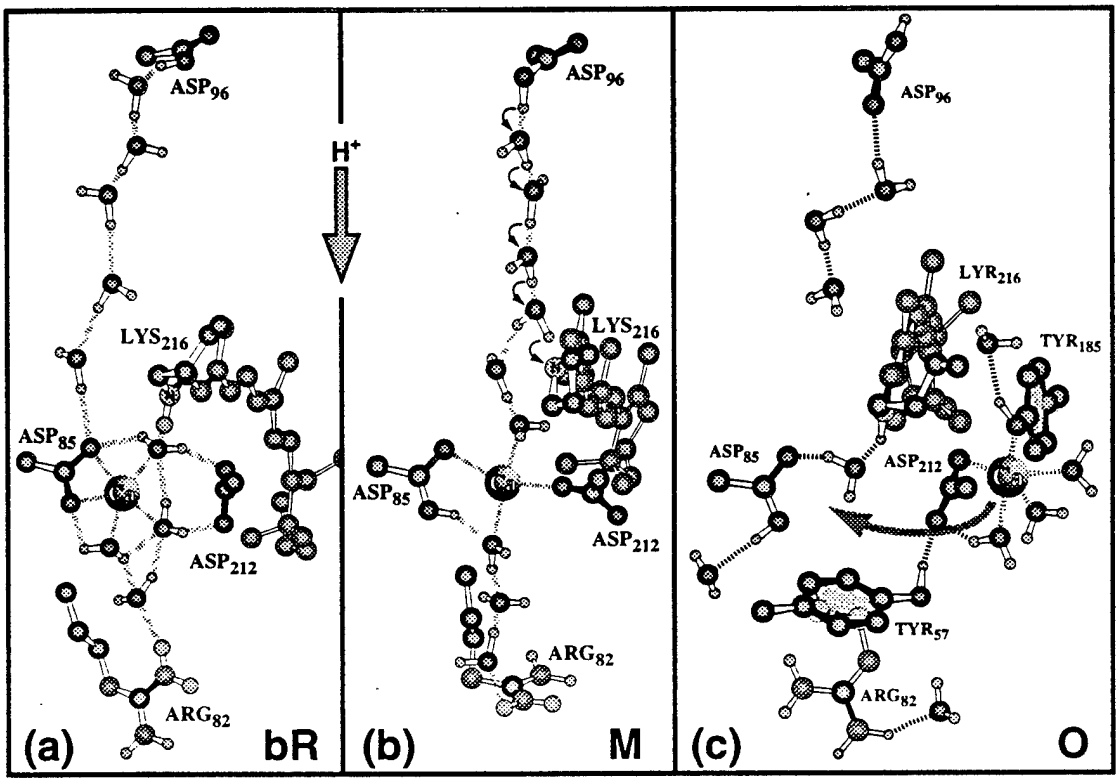

Figure 12. Molecular models of the **bR**, **M** and **O** states of bacteriorhodopsin showing the chromophore, selected amino acid residues and the near-chromophore calcium binding site. Direction towards the cytoplasmic and extracellular surfaces and the proton pumping vector are indicated. Microwave absorptivity experiments suggest that in native **bR**, the calcium enters the proton channel and provides an electrostatic gate preventing back transfer of the proton during the latter stages of the photocycle [34]. The arrow in the **O** state diagram indicates the migration of the cation back to its native position during the **O** → **bR** reaction.

We close with a brief explanation of how we believe the organic cations are affecting the yield of the **O** state. Molecular modeling suggests that the **O** → **bR** reaction requires a migration of the cation (calcium in the native protein) as shown in Fig. 12. Thus, as the molecular weight of the cation increases, the decay of the **O** state is slowed. Thus, an increase in molecular weight of the cation will increase the yield of the **O** state for kinetic reasons. However, at some point the cation becomes too large to occupy the native cation binding site, and thus an alternative site is found that is less restrictive. We believe this site is closer to the cation binding site shown for **bR** (see discussion of the two models of the **O** state cation binding sites in Ref. [34]). Thus, there is a maximum in the yield versus molecular weight graph (Fig. 11b).

7. Comments and Conclusions

The branched-photocycle optical memory described above shows considerable potential, but much remains to be accomplished before we can view this architecture as competitive with other architectures under development and within the commercial sector. The following work is being performed under our current Rome Laboratory contract to more fully examine and enhance the potential of the bacteriorhodopsin-based branched-photocycle three-dimensional memory.

The prototype shown in Fig. 4 is being redesigned to permit the use of commercially available laser diodes, CCD array detectors and active matrix spatial light modulators. The goal is to make a small-scale level II prototype to explore more fully the commercial viability of our architecture, examine better methods of paging and test new protein analogs developed in the latter stages of this contract. We are also working with DuPont and other companies to explore new polymer matrices which may offer improvements in homogeneity and optical clarity. Scattering of light within the data cuvette remains an important issue that has not been fully resolved. Finally, we note that our current method of paging is inefficient with respect to optical resolution, because the light is entering from only one side of the data cuvette. We will explore the use of two laser diodes operating at 635 nm each focused to produce diffraction-limited thin line paging beams with the two beams entering from opposite sides of the cuvette. This design will permit higher density operation. We are also exploring various alignment verification techniques, which are required to position the data cuvette so that the memory device can reproducibly go to a designated page with sufficient accuracy. This is a critical requirement for high-density diffraction limited performance.

The protein bacteriorhodopsin has many characteristics that are near-optimal for use in the branched-photocycle architecture. However, it is unrealistic to expect that nature has optimized the protein for this particular application, and we will continue our investigation of chemically and genetically modified bacteriorhodopsin proteins to identify candidates that improve performance. While the organic cation analog proteins show great promise, we have not fully evaluated the potential of site-directed mutagenesis to enhance the branching photochemistry. Through a collaboration with Prof. Richard Needleman, we are initiating a study of selected mutants with extended **O** state lifetimes and yields to determine the impact of these mutations on the performance of the protein in the branched-photocycle architecture.

Finally, the homogeneity of the memory medium requires improvement. While polyacrylamide provides excellent protein stability, the small cavities that are created following polymerization provide scattering centers that limit resolution and the quality of the read signal image. DuPont Corporation has offered to help us identify new polymers that will provide adequate stabilization of the protein while improving homogeneity of the data cuvettes. Hybrid polymers involving various combinations of polyvinyl alcohol and gelatin will be investigated.

8. References.

1. M.A. El-Sayed, On the molecular mechanisms of the solar to electric energy conversion by the other photosynthetic system in nature, bacteriorhodopsin, *Accts. Chem. Res.* **25**, 279-286 (1992).

2. J.K. Lanyi, Bacteriorhodopsin as a model for proton pumps, *Nature* **375**, 461-463 (1995).

3. R.A. Mathies, S.W. Lin, J.B. Ames and W.T. Pollard, From femtoseconds to biology: Mechanism of bacteriorhdopsin's light-driven proton pump, *Annu. Rev. Biophys. Biophys. Chem.* **20**, 491-518 (1991).

4. K.J. Rothschild, FTIR difference spectroscopy of bacteriorhodopsin: toward a molecular model, *J. Bioenerg. Biomembr.* **24**, 147-167 (1992).

5. R.R. Birge, Photophysics and molecular electronic applications of the rhodopsins, *Annu. Rev. Phys. Chem.* **41**, 683-733 (1990).

6. R.A. Mathies, C.H. Brito Cruz, W.T. Pollard and C.V. Shank, Direct observation of the femtosecond excited-state cis-trans isomerization in bacteriorhodopsin, *Science* **240**, 777 (1988).

7. Y. Shen, C.R. Safinya, K.S. Liang, A.F. Ruppert and K.J. Rothschild, Stabilization of the membrane protein bacteriorhodopsin to 140°C in two-dimensional films, *Nature* **366**, 48-50 (1993).

8. D. Oesterhelt, C. Bräuchle and N. Hampp, Bacteriorhodopsin: a biological material for information processing, *Quart. Rev. Biophys.* **24**, 425-478 (1991).

9. R.R. Birge, Protein based optical computing and optical memories, *IEEE Computer* **25**, 56-67 (1992).

10. R.R. Birge, Three-dimensional optical memories, *Amer. Sci.* **82**, 349-355 (1994).

11. R.R. Birge, Protein-based computers, *Scientific American* **272**, 90-95 (1995).

12. A. Popp, M. Wolperdinger, N. Hampp, C. Bräuchle and D. Oesterhelt, Photochemical conversion of the O-intermediate to 9-cis-retinal-containing products in bacteriorhodopsin films, *Biophys. J.* **65**, 1449-1459 (1993).

13. D.A. Parthenopoulos and P.M. Rentzepis, Three-dimensional optical storage memory, *Science* **245**, 843-845 (1989).

14. M.E. Marhic, Storage limit of two-photon-based three-dimensional memories with parallel access, *Optics Lett.* **16**, 1272-1273 (1991).

15. A.S. Dvornikov and P.M. Rentzepis, Two photon three-dimensional optical storage memory, *Adv. Chem.* **240**, 161-178 (1994).

16. S. Hunter, F. Kiamilev, S. Esener, D.A. Parthenopoulos and P.M. Rentzepis, Potential of two-photon based 3-D optical memories for high performance computing, *Appl. Opt.* **29**, 2058-2066 (1990).

17. J.F. Heanue, M.C. Bashaw and L. Hesselink, Volume holographic storage and retrieval of digital data, *Science* **265**, 749-752 (1994).

18. K. Curtis and D. Psaltis, Recording of multiple holograms in photopolymer films, *Appl. Opt.* **31**, 7425-7428 (1992).

19. E.G. Paek and D. Psaltis, Optical associative memory using Fourier transform holograms, *Opt. Eng.* **26**, 428-433 (1987).

20. Z. Chen, D. Govender, R. Gross and R. Birge, Advances in protein-based three-dimensional optical memories, *BioSystems* **35**, 145-151 (1995).

21. R.R. Birge and C.F. Zhang, Two-photon spectroscopy of light adapted bacteriorhodopsin, *J. Chem. Phys.* **92**, 7178-7195 (1990).

22. J.A. Stuart, B.W. Vought, C.F. Zhang and R.R. Birge, The active site of bacteriorhodopsin. Two-photon spectroscopic evidence for a positively charged chromophore binding site mediated by calcium, *Biospectroscopy* **1**, 9-28 (1995).

23. R.R. Birge, R.B. Gross, M.B. Masthay, J.A. Stuart, J.R. Tallent and C.F. Zhang, Nonlinear optical properties of bacteriorhodopsin and protein based two-photon three-dimensional memories, *Mol. Cryst. Liq. Cryst. Sci. Technol. Sec. B. Nonlinear Optics* **3**, 133-147 (1992).

24. A.F. Lawrence and R.R. Birge, The potential application of optical phased arrays in two-photon three-dimensional optical memories, *Proc. SPIE* **1773**, 401-412 (1992).

25. R.R. Birge and D.S.K. Govender, *Three-dimensional optical memory*, U.S. Patent Number 5,253,198; October 12, 1993, Syracuse University,

26. B.M. Becher and J.Y. Cassim, Improved isolation procedures for the purple membrane of Halobacterium halobium, *Prep. Biochem.* **5**, 161-178 (1975).

27. D. Hames, One-dimensional polyacrylamide gel electrophoresis, in *Gel electrophoresis of proteins: a practical approach* vol. IRL Press, Oxford, (1990)

28. G. Varo and J.K. Lanyi, Thermodynamics and energy coupling in the bacteriorhdopsin photocycle, *Biochem.* **30**, 5016-5022 (1991).

29. G. Varo and J.K. Lanyi, Effects of the crystalline structure of purple membrane on the kinetics and energetics of the bacteriorhodopsin photocycle, *Biochem.* **30**, 7165-7171 (1991).

30. Y.N. Zhang, M.A. El-Sayed, M.L. Bonet, J.K. Lanyi, M. Chang, B. Ni and R. Needleman, Effects of genetic replacements of charged and H-bonding residues in the retinal pocket on Ca^{2+} binding to deionized bacteriorhodopsin, *Proc. Natl. Acad. Sci. USA* **90**, 1445-1449 (1993).

31. Y.N. Zhang, L.L. Sweetman, E.S. Awad and M.A. El-Sayed, Nature of the individual Ca^{2+} binding sites in Ca^{2+}-regenerated bacteriorhodopsin, *Biophys. J.* **61**, 1201-1206 (1992).

32. E.H.L. Tan, D.S.K. Govender and R.R. Birge, Large organic cations can replace Mg^{2+} and Ca^{2+} ions in bacteriorhodopsin and maintain proton pumping ability, *J. Am. Chem. Soc.* **118**, 2752-2753 (1996).

33. F.M. Menger and S. Wrenn, Interfacial and micellar properties of molaform electrolytes, *J. Phys. Chem.* **78**, 1387-1390 (1974).

34. R.R. Birge, D.S.K. Govender, K.C. Izgi and E.H.L. Tan, Role of calcium in the proton pump of bacteriorhodopsin. Microwave evidence for a cation-gated mechanism, *J. Phys. Chem.* 9990-10004 (1996).

9. Publications Sponsored in Part by This Contract:

1. R.R. Birge, Three-dimensional optical memories, *Amer. Sci.* **82**, 349-355 (1994).

2. R.R. Birge, Bacteriorhodopsin, in *Encyclopedia of Advanced Materials* (eds. D. Bloor), vol. Pergamon, Oxford, UK, (1994) pp. 199-204.

3. Q.W. Song, C. Zhang, R.B. Gross and R.R. Birge, The intensity-dependent refractive index of chemically enhanced bacteriorhodopsin, *Optics Commun.* **112**, 296-301 (1994).

4. C. Zhang, Q.W. Song, C.Y. Ku, R.B. Gross and R.R. Birge, Determination of the refractive index of a bacteriorhodopsin film, *Optics Letters* **19**, 1406-1411 (1994).

5. R.R. Birge, D.S.K. Govender, R.B. Gross, A.F. Lawrence, J.A. Stuart, J.R. Tallent, E. Tan and B.W. Vought, Bioelectronics, three-dimensional memories and hybrid computers. *IEEE IEDM Technical Digest* **94**, 3-6 (1994).

6. R.R. Birge and R.B. Gross, Biomolecular optoelectronics, in *Introduction to Molecular Electronics* (eds. M.C. Petty, M.R. Bryce and D. Bloor), vol. Edward Arnold, London, (1995) pp. 315-344.

7. R.R. Birge, Z. Chen, D. Govender, R.B. Gross, S.B. Hom, K.C. Izgi, J.A. Stuart and B.W. Vought, Biomolecular photonics based on bacteriorhodopsin, *CRC Handbook of Organic Photochemistry Photobiolology* 1568-1587 (1995).

8. Q.W. Song, C. Zhang, C.Y. Ku, M.C. Huang, R.B. Gross and R.R. Birge, Determination of the thermal expansion and thermo-optical coefficients of a bateriorhodopsin film, *Optics Commun.* **115**, 471-474 (1995).

9. R.R. Birge, Protein-based computers, *Scientific American* **272**, 90-95 (1995).

10. R.B. Gross, A.T. Todorov and R.R. Birge, The wavelength-dependent refractive index change associated with the blue to pink membrane photochemical conversion in bacteriorhodopsin, in *Applications of Photonic Technology* (eds. G.A. Lampropoulos), vol. Plenum Press, New York, (1995) pp. 115-121.

11. Y.H. Zhang, Q.W. Song, C. Tseronis and R.R. Birge, Real-time holographic imaging with a bacteriorhodopsin film, *Optics Letters* **20**, 2429-2431 (1995).

12. Q.W. Song, C.Y. Ku, R.B. Gross, R.R. Birge and R. Michalak, Modified critical angle method for measuring the refractive index of bio-optical materials and its application to bacteriorhodopsin, *J. Opt. Soc. Amer. B.* **12**, 797-803 (1995).

13. Z. Chen, D. Govender, R. Gross and R. Birge, Advances in protein-based three-dimensional optical memories, *BioSystems* **35**, 145-151 (1995).

14. E.H.L. Tan, D.S.K. Govender and R.R. Birge, Large organic cations can replace Mg^{2+} and Ca^{2+} ions in bacteriorhodopsin and maintain proton pumping ability, *J. Am. Chem. Soc.* **118**, 2752-2753 (1996).

15. R.R. Birge, D.S.K. Govender, K.C. Izgi and E.H.L. Tan, Role of calcium in the proton pump of bacteriorhodopsin. Microwave evidence for a cation-gated mechanism, *J. Phys. Chem.* 9990-10004 (1996).

16. J.A. Stuart, J.R. Tallent, E.H.L. Tan and R.R. Birge, Protein-based volumetric memory, *Proc. IEEE Nonvol. Mem. Tech. (INVMTC)* **6**, 45-51 (1996).

10. Patents

Patent 2 was based on previous Rome Laboratories contracts. Patent 3 was based on this contract (F30602-93-C-0135).

1. Optical random access memory. R.R. Birge and A.F. Lawrence, U.S. Patent Number 5,228,001; July 13, 1993.

2. Three-Dimensional Optical Memory. R.R. Birge and D.S.K. Govender, U.S. Patent Number 5,253,198; October 12, 1993.

3. Branched-Photocycle Volumetric Memory. R.R. Birge, (patent approved).

MISSION OF ROME LABORATORY

Mission. The mission of Rome Laboratory is to advance the science and technologies of command, control, communications and intelligence and to transition them into systems to meet customer needs. To achieve this, Rome Lab:

a. Conducts vigorous research, development and test programs in all applicable technologies;

b. Transitions technology to current and future systems to improve operational capability, readiness, and supportability;

c. Provides a full range of technical support to Air Force Material Command product centers and other Air Force organizations;

d. Promotes transfer of technology to the private sector;

e. Maintains leading edge technological expertise in the areas of surveillance, communications, command and control, intelligence, reliability science, electro-magnetic technology, photonics, signal processing, and computational science.

The thrust areas of technical competence include: Surveillance, Communications, Command and Control, Intelligence, Signal Processing, Computer Science and Technology, Electromagnetic Technology, Photonics and Reliability Sciences.